Posted on 8 Aug 2023 — The copyright holder is the author/funder. All rights reserved. No reuse without permission. — https://doi.org/10.22541/essoar.169149923.32348420/v1 — This a preprint and has not been peer reviewed. Data may be preliminary.

Deep Short-term Slow Slip and Tremor in the Manawatu Region, New Zealand

Shannon Lee Fasola[1], Noel McCay Jackson[1], and Charles A. Williams[2]

[1]University of Kansas
[2]GNS Science

August 8, 2023

Abstract

The Manawatu region experiences deep tremor and long-term SSEs; however tremor is adjacent to, and not co-located with, long-term SSEs. Observations of Episodic tremor and Slip (ETS) elsewhere suggest it is possible smaller short-term SSEs below the current detection threshold occur where tremor is observed. Therefore, we sought to determine if small SSEs occurred with Manawau tremor. We decomposed GNSS data using times of tremor to assess average surface displacements and performed a static slip inversion to model the displacement during tremor. The slip inversion suggested small slow slip partially coincided with tremor and long-term SSEs may influence these small SSEs by increasing slip rates. We suggest that the interface below deep long-term SSEs may slip often, in small ETS-like SSEs that are not individually detectable geodetically. The question remains as to the nature of the strong variability in SSE behavior with depth and duration in the southern Hikauangi margin.

Hosted file

968428_0_art_file_11205447_ry1yfb.docx available at https://authorea.com/users/641746/articles/655872-deep-short-term-slow-slip-and-tremor-in-the-manawatu-region-new-zealand

Deep Short-term Slow Slip and Tremor in the Manawatu Region, New Zealand

Shannon L. Fasola[1], Noel M. Jackson[1], and Charles A. Williams[2]

[1]Department of Geology, University of Kansas, Lawrence, KS.

[2]GNS Science, Lower Hutt, New Zealand.

Corresponding author: Shannon Fasola (shannon.fasola@ku.edu)

Key Points:

- GNSS data indicates newly detected short-term slow slip in region of deep tremor
- Long-term slow slip events may influence these small slow slip events by increasing slip rates
- Three types of slow slip overlap along-strike in Hikuragni margin: shallow, short-term; deep, long-term; deeper, short-term with tremor

Abstract

The Manawatu region experiences deep tremor and long-term SSEs; however tremor is adjacent to, and not co-located with, long-term SSEs. Observations of Episodic tremor and Slip (ETS) elsewhere suggest it is possible smaller short-term SSEs below the current detection threshold occur where tremor is observed. Therefore, we sought to determine if small SSEs occurred with Manawau tremor. We decomposed GNSS data using times of tremor to assess average surface displacements and performed a static slip inversion to model the displacement during tremor. The slip inversion suggested small slow slip partially coincided with tremor and long-term SSEs may influence these small SSEs by increasing slip rates. We suggest that the interface below deep long-term SSEs may slip often, in small ETS-like SSEs that are not individually detectable geodetically. The question remains as to the nature of the strong variability in SSE behavior with depth and duration in the southern Hikauangi margin.

Plain Language Summary

In between the Earth's tectonic plates, energy builds over time and can be released along faults suddenly (seconds-minutes; i.e., earthquakes) or slowly (weeks-years; i.e., slow slip events). Slow slip often happens with low-frequency earthquakes (i.e., tectonic tremor). The North Island, New Zealand features two colliding tectonic plates with the potential to generate large earthquakes. The interface between these plates has both deep tectonic tremor and large, long-lasting slow slip, but the tectonic tremor is deeper on the fault than the large slow slip. Studies have suggested small, short-lasting slow slip, usually not able to be detected, occur where tectonic tremor is found. In this study we tried a different approach to find the small slow slip. While small slow slip are not detected by themselves, we were able to detect their cumulative effect in the tectonic tremor area. We modeled small slow slip during tectonic tremor to find the mean sliding rate on the fault that is between the tectonic plates. The large long-lasting slow slip may drive these smaller slow slip by making them slip faster. The question remains as to the cause of the many types of slow slip in New Zealand.

1 Introduction

Tectonic tremor was first detected in the Nankai subduction zone in southwest Japan (Obara, 2002) and has since been discovered in several subduction zones around the world.

Tectonic tremor consists of low-level seismic vibrations representing a swarm of low-frequency earthquakes (Brown et al., 2009; Ide et al., 2007; Shelly et al., 2006, 2007). Tremor is often accompanied by and thought to be the result of slow slip events (SSEs; Bartlow et al., 2011; Shelly et al., 2006; Wech & Creager, 2007). As a result, tremor is thought to be a proxy for slow slip, and hence can be used to track and better understand SSEs. These aseismic ruptures occur on the plate interface in the frictional transition zone from stick-slip to stable sliding (Beroza & Ide, 2011; Dragert et al., 2001) or in zones of high pore fluid pressure and low effective stress (e.g. Gao & Wang, 2017; Hyndman et al., 2015). While the amount of strain released from tremor is relatively small, SSEs are capable of releasing as much strain along the plate interface as M 7+ earthquakes (e.g., Radiguet et al., 2012). There have also been cases where SSEs have been found to precede large megathrust earthquakes (e.g., Graham et al., 2014; Kato et al., 2012; Ruiz et al., 2014). Therefore, understanding the behavior of slow slip and tremor is valuable for estimating its potential impact on the seismic budget (e.g., Obara & Kato, 2016; Radiguet et al., 2016) and potential for triggering future earthquakes.

There are a variety of scenarios in which tremor occurs with slow slip. Tremor that spatiotemporally correlates with short-term SSEs is referred to as “episodic tremor and slip” (ETS) which is prominent in the Nankai and Cascadia subduction zones at depths of 25–45 km (Obara et al., 2004; Rogers & Dragert, 2003). Tremor is not always co-located with SSEs, but is instead found offset downdip from the region of slow slip as in the Bungo Channel in Japan and Costa Rica (Brown et al., 2009; Hirose et al., 2010). Bursts of tremor co-located with or near the down-dip limit of long-term SSEs have also been detected in Mexico, Alaska, and Japan, with a higher frequency of tremors during long-term SSEs (Frank et al., 2018; Hirose et al., 2010; Rousset et al., 2019). Frank et al. (2018) and Rousset et al. (2019) both suggested that long-term SSEs were actually composed of a cluster of short ETS-like events while Rousset et al. (2019) also proposed the long-term SSE may have occurred updip from a cluster of short ETS-like events. The difference in the variability in tremor behavior within and between subduction zones is not well understood. Therefore, it is important to study tremor and slow slip in as many regions as possible to evaluate the full range of behaviors.

The North Island of New Zealand along the Hikurangi margin provides an excellent opportunity to further investigate the wide range of tremor and slow slip behaviors. New Zealand has both shallow, short-term SSEs and deep, mid- to long-term SSEs. See Wallace (2020) for a

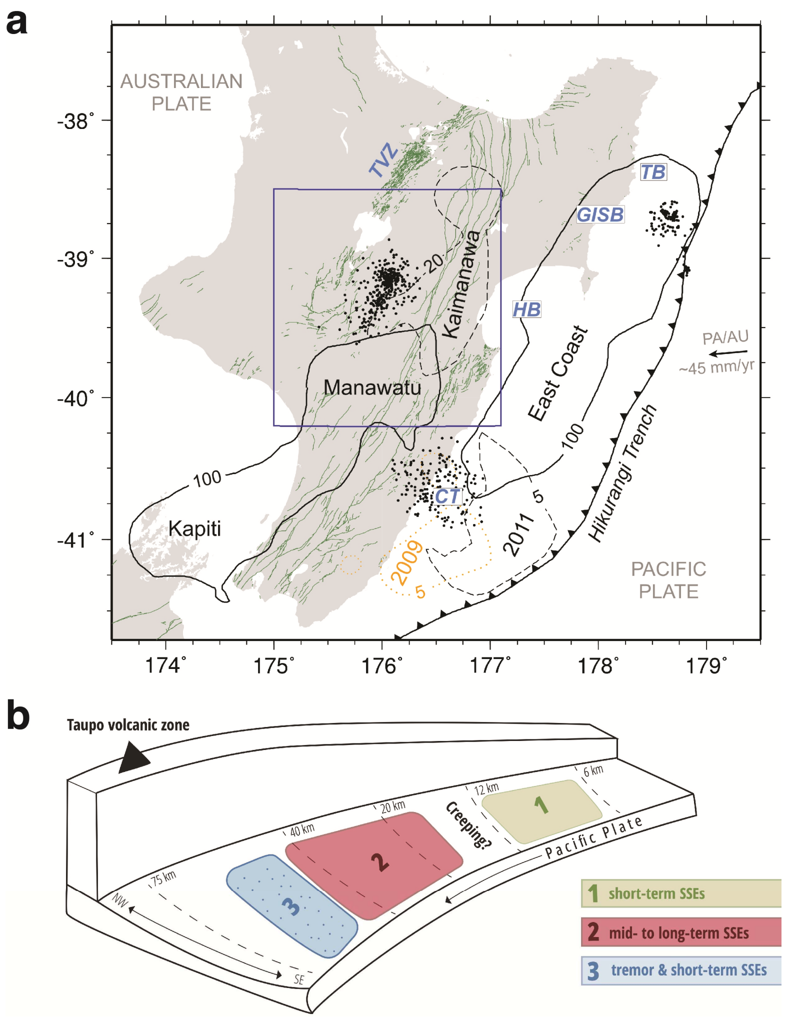

Figure 1. a. Slow slip and tectonic tremor for North Island, New Zealand. Cumulative slip (mm) for 2002-2014 in Kapiti, Manawatu and East Coast SSEs (solid line; Wallace, 2020), 2006 and 2008 Kaimanawa SSEs (dashed line; Wallace, 2020), 2011 Cape Turnagain SSE (dashed line; Bartlow et al., 2014), and small 2009 SSE (orange dotted line; Wallace, 2020; Wallace, Barnes, et al., 2012). Tectonic tremor (2005-2016) is represented by black dots (Manawatu and Cape Turnagain: Romanet & Ide, 2019; Gisborne: Todd et al., 2018). Faults (green lines; Langridge et al., 2016), Pacific-Australia relative plate motion (arrow; Beavan et al., 2002), and study region (blue box) are marked. Abbreviations: Cape Turnagain, CT; Gisborne, GISB; Hawkes Bay, HB; Tolga Bay, TB; Taupo volcanic zone, TVZ. b. Sketch of the tremor and slip dynamics in the Manawatu region.

detailed review of New Zealand's SSEs. Tremor has been observed with shallow SSEs near Gisborne and Cape Turnagain (e.g. Romanet & Ide, 2019; Todd et al., 2018) and downdip of deep SSEs near Manawatu (Romanet & Ide, 2019). However, most SSEs in New Zealand are not accompanied by observed tectonic tremor. Instead, increased rates of seismicity are more commonly associated with SSEs at the Hikurangi margin (e.g., Bartlow et al. 2014; Delahaye et al. 2009; Jacobs et al. 2016; Reyners & Bannister 2007; Shaddox & Schwartz 2019; Yarce et al. 2019). Wallace (2020) suggested the difference in the more dominant seismic signature could reflect the thermal structure of the subduction zone (Yabe et al., 2014), frictional heterogeneities in the region of slow slip (Wallace, Barnes, et al. 2012), and attenuation within the upper plate that would impact the ability of tremor to be recorded at the surface (Todd & Schwartz, 2016).

In this study, we focused on the deep portion of the central Hikurangi margin where large (M_W 6.9-7.2), long-term (1-2 year) Manawatu SSEs and small (M_W 6.6), mid-term (couple months) Kaimanawa SSEs occur at similar depth but are adjacent to each other along-strike (Figure 1) (Wallace, 2020). Tremor occurs down dip from the Manawatu and Kaimanawa SSEs and both during and in between times of SSEs (Romanet & Ide, 2019). Observations of ETS elsewhere in the world and more frequent tremor episodes relative to the mid- to long-term deep SSEs at the Hikurangi margin suggest it is possible smaller short-term SSEs below the current geodetic network detection threshold also occur in the area of observed tremor. This would indicate SSEs occur at three different depth ranges in the central Hikurangi margin. Therefore, we sought to further investigate tremor in the Manawatu region to determine if a detectable geodetic signal can be identified with decomposition, in which we stacked tremor displacement offsets on GNSS time series and calculated a time-averaged displacement rate. Time-averaged displacement rates during tremor periods were then compared with displacement rates outside of tremor periods and inverted to obtain a model of slip rate on the plate interface associated with tremor. It is valuable to understand how much of the seismic budget is being released aseismically and to what degree, if any, do the different types of SSEs impact each other. This study seeks to build on the understanding of the already complex nature of SSEs and tremor at the Hikurangi margin.

2 Data and Methods

For this study we used daily time-series solutions from continuous GNSS stations from the GeoNet network on the North Island (GNS Science, 2000). GNSS time series were referenced to the fixed Australian plate, and outliers and offsets due to antenna changes and earthquakes were removed. Time series were regionally filtered by removing a common mode signal (Figure S1). See supporting information for more details on post-processing of the time series.

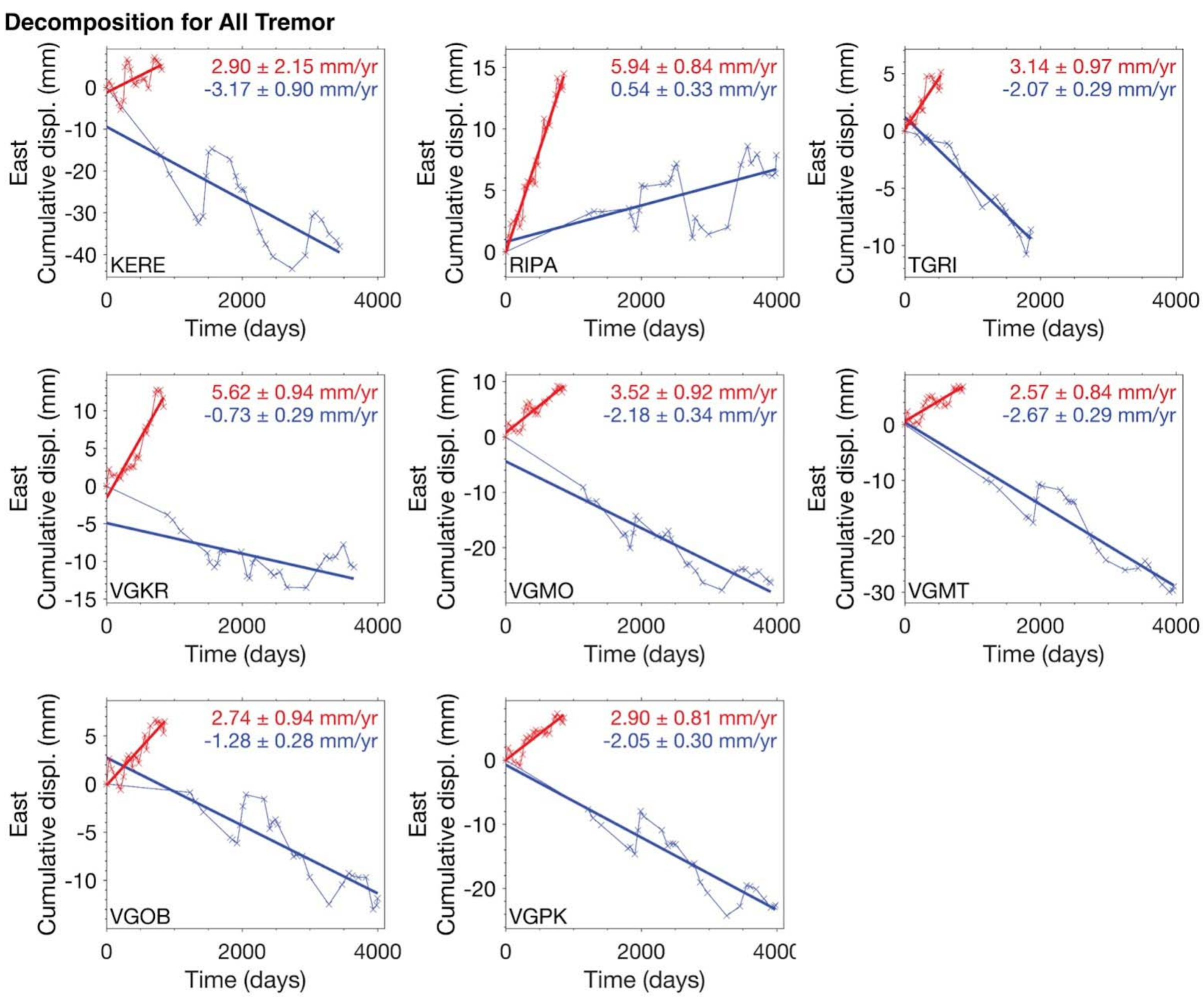

Figure 2. Decomposition of the East components of the entire time series for stations whose decompositions were found to be robust. Red and blue curves indicate cumulative offsets during tremor and inter-tremor periods, respectively. Values represent velocities from a best-fit line and 1σ uncertainties obtained from random resampling. See Figure S3 for east and north components for all stations used in the inversion.

We decomposed the GNSS time series in the Manawatu region based on times of tremor following the methods of Rousset et al. (2019). We used the tremor catalog from Romanet and Ide (2019) which spans from 2005 through 2016 and consists of 354 events in the Manawatu region. Therefore, time series used for decomposition ranged from 2005, or the start of station recording, until the day before the 14 November 2016 M_W 7.8 Kaikoura earthquake in order to avoid signals from the earthquake. Twelve GNSS stations surrounding the Manawatu tremor were used for decomposition which had no large gaps in data and were recording for at least two deep, mid- to long-term SSEs. We acknowledge that there are stations near the tremor that were not used for decomposition (Figure S1d). It is important to note that part of this region overlaps with the Taupo volcanic zone and there are multiple stations directly on volcanoes. Thus, we sought to limit the use of volcanic stations to avoid any volcanic signals.

Tremor was grouped into clusters to identify bursts of tremor which are believed to represent transient slip (Frank et al., 2018; Hawthorne & Rubin, 2013; Villafuerte & Cruz-Atienza, 2017). As in Rousset et al. (2019), we used daily counts of tremor detections and grouped them into clusters based on a 22-day minimum inter-cluster duration and minimum number of 5 events per cluster (Figure S2). Due to the smaller tremor catalog relative to those in other studies applying the decomposition method, we first utilized every tremor burst when decomposing the GNSS time series without distinguishing whether the burst occurred during or in between identified deep SSEs. For each tremor cluster, we estimated the corresponding displacement in the GNSS time series horizontal components by computing the difference between average positions 10 days after and before each cluster. Displacements and durations of each tremor cluster were stacked to produce a time series of cumulative displacement increments for both horizontal components on each station (Figure 2, S3). Similarly, cumulative displacement increments during the inter-tremor period (i.e., times of no tremor) were measured. We performed a linear regression to the tremor and inter-tremor displacement time series to find time-averaged displacement rates (i.e., time-averaged velocities). Tremor and inter-tremor velocity vectors were plotted to obtain a sense of direction and to confirm that vectors were spatially coherent (Figure 3a). To find the true tremor velocity, we isolated the tremor signal by subtracting the inter-tremor velocity from the velocity during the tremor period (Figure 3b). Essentially, we removed the plate convergence rate, the slip associated with mid- to long-term SSEs but not associated with times of tremor, and any other long-term signals from the tremor signal by subtracting out the inter-tremor velocity such that the new tremor velocities were relative to an 'inter-tremor motion' fixed reference. In discussing the results of this study, we will refer to the true tremor velocities in the 'inter-tremor motion' fixed reference frame as simply the ‘tremor velocities’. The uncertainty of the velocities was determined by taking the standard deviation from the population of velocities generated through random resampling of the displacement increments.

We sought to determine if tremor-associated motions were affected by the deep mid- to long-term SSEs in the Manawatu and Kaimanawa regions. We computed time-averaged tremor and inter-tremor velocities only during the mid- to long-term SSEs via decomposition (Figure S4-S5). The deep SSEs during the time frame analyzed were the 2004-2005, 2010-2011, 2014-2015 Manawatu SSEs and the 2006, 2008, 2013 Kaimanawa SSEs (Figure S2) (Bartlow et al., 2014; Wallace, 2020; Wallace & Beavan, 2010; Wallace & Eberhart-Phillips, 2013). Wallace and Eberhart-Phillips (2013) identified a shallow SSE in February-March 2013, 20 km updip from the 2006 and 2008 Kaimanawa SSEs. However, there may have also been a deep SSE during this time similar to the 2006 and 2008 mid-term Kaimanawa SSEs (personal communication with Laura Wallace). Therefore, we included this probable deep 2013 event as a SSE during the decomposition. We also computed time-averaged tremor and inter-tremor velocities during the inter-SSEs periods (Figure S6-S7). In order to quantify the robustness of these decompositions with regard to background noise levels, we followed the modified bootstrapping approach of Rousset et al. (2019) (Figures S8-10). See supporting information for more details on determining robustness of the decompositions.

3 Results

The direction of the time-averaged tremor velocities obtained from all clusters for stations closest to the tremor were spatially coherent and oriented southeast consistent with slip on the plate interface (Figure 3b). Tremor velocities were negligible at far-field stations and only significant at stations closest to the Manawatu tremor as we would expect (Figure 3b). This supports that the decomposition method was able to detect a geodetic signal associated with the tremor. With the exception of the stations updip of the tremor, the magnitude of the tremor displacement rates was larger than those during the inter-tremor periods suggesting the plate interface below stations within and downdip from the tremor was slipping faster than during times of no tremor. Time-averaged tremor surface displacement rates ranged from 3-7 mm/yr.

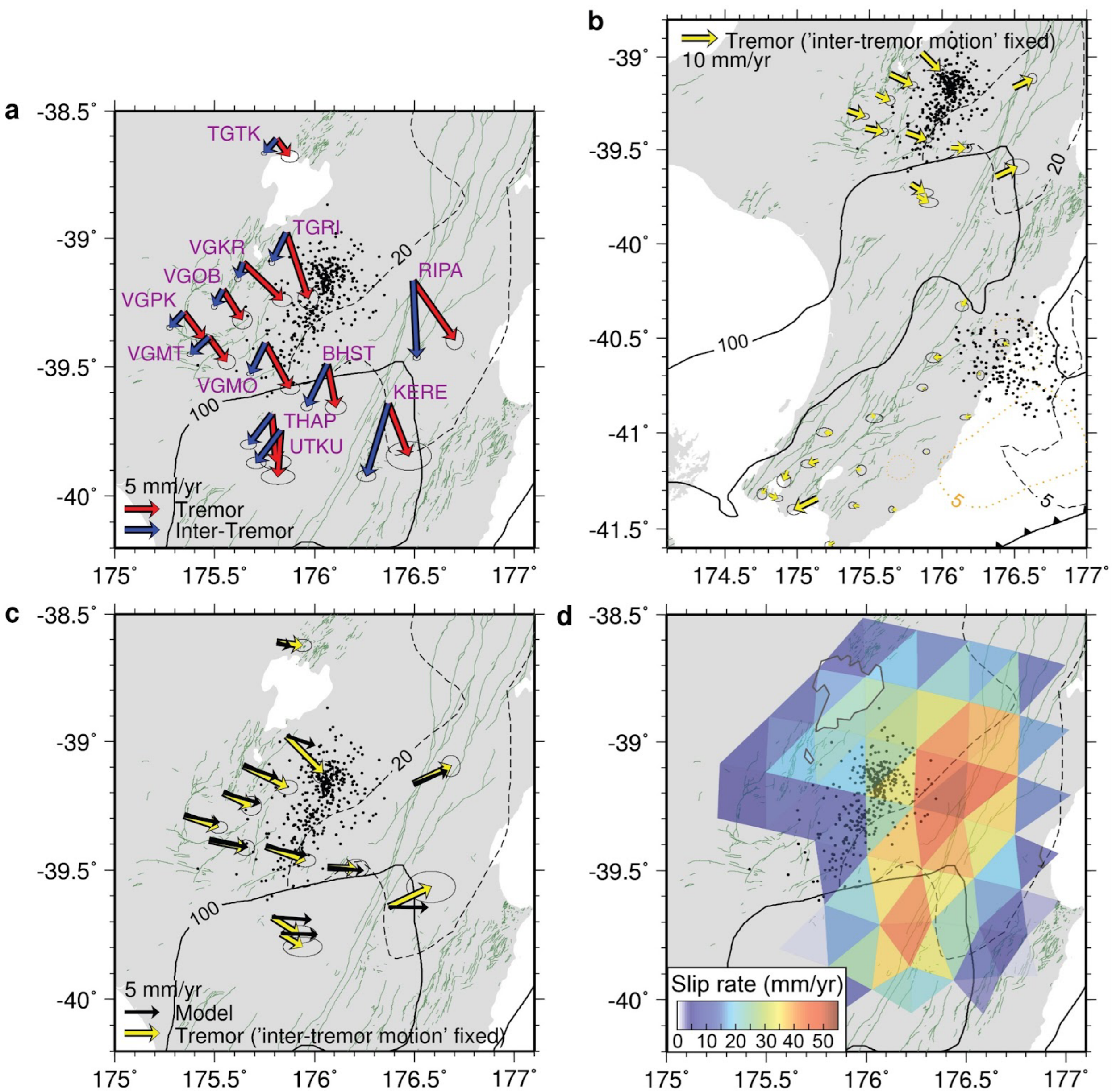

Figure 3. Time-averaged displacement rate and slip rate for all tremor bursts. a) Displacement rate of tremor (red arrows) and inter-tremor periods (blue arrows) with 1σ uncertainties are shown. GeoNet GNSS station names are in purple. b) A zoomed out view of true tremor displacement rates with the 'inter-tremor motion' fixed (yellow arrows) and 1σ uncertainty. c) Comparison of the true tremor displacement rates (yellow arrows) and modeled tremor displacement rates (black arrows). d) Time-averaged slip rate during tremor bursts as estimated by static slip inversion.

For tremor that occurred during the deep, mid- to long-term Manawatu and Kaimanawa SSEs, we also saw a coherent signal among stations closest to the tremor with all but two stations oriented towards the trench (Figure S5). The magnitude of tremor displacement rates were larger than those when considering the entire tremor catalog suggesting a potential influence of the deep SSEs. Tremor displacement rates during deep SSEs ranged from 5-10 mm/yr. The tremor signal was not as spatially coherent for tremor during the inter-SSE period and was very small (1-4 mm/yr) yet still visible at some stations (Figure S7). The lack of a spatially coherent tremor signal during the inter-SSE period is likely a result of the weak robustness of the decomposition for the inter-SSE period (Figure S10).

3.1 Static Slip Inversion

We used a weighted, Laplacian smoothed, nonnegative least squares inversion with heterogeneous Green's functions to invert the time-averaged tremor velocities (Figure 3) for tremor-associated slip rate on the plate interface. We used a triangular mesh to represent the fault surface, using the Hikurangi fault geometry of Williams et al. (2013). We embedded the fault geometry within a tetrahedral volume mesh and used the finite element code PyLith (Aagaard et al., 2013, 2017a, 2017b) to generate Green's functions for the observation sites. By using PyLith to generate our Green's functions, we were able to account for elastic heterogeneity using the New Zealand-wide seismic velocity model (Eberhart-Phillips et al., 2010; Eberhart-Phillips & Bannister, 2015; Eberhart-Phillips & Reyners, 2012; Reyners et al., 2014). As shown by Williams and Wallace (2015, 2018), accounting for elastic heterogeneity typically has a large effect on slip; for deep events, accounting for elastic heterogeneity decreases estimated slip by about 20%. Slip direction was specified for each triangle using the tectonic block model of Wallace, Beavan et al. (2012).

Both the data and Green's functions were weighted with the inverse of the tremor velocity uncertainties. Smoothing was applied by appending a discrete Laplacian matrix onto the Green's function matrix and zeros to the data vector. The Laplacian matrix was scaled by the Green's function amplitudes and multiplied by a smoothing parameter of 16, selected by visual inspection of an L-curve (Figure S11). MATLAB's nonnegative least squares function (lsqnonneg) was used to impose nonnegativity, preventing reversal of slip of the plate interface. For specifics on the inversion, see Bartlow (2020). The resulting slip rate estimates should be considered time-averaged estimates of tremor slip rate, which are not applicable to a single tremor cluster. The time-averaged tremor velocities during SSE and inter-SSE periods were also inverted. We calculated a total moment rate for each of the three modeled slip rate solutions and estimated the average moment per tremor burst (Table S1). For details on the moment rate calculation, see the supplement.

Inverting the time-averaged tremor displacement rates considering all tremor clusters revealed tremor-associated slip co-located with the tremor and in the Manawatu and Kaimanawa SSE source regions (Figure 3d). Maximum slip rates were 45-50 mm/yr and updip from the region of tremor, coinciding with the downdip edge of the Kaimanawa SSEs. There was a second slip rate maximum, ~40 mm/yr, which coincided with the Manawatu SSE source region. Slip rates in the tremor region were 10-30 mm/yr. The total moment rate for the entire slip area was 2.4×10^{19} Nm/yr, while the average moment per tremor burst was 1.5×10^{18} Nm equivalent to a M_W 5.0.

Decomposition for the SSE period revealed periods of fast slip associated with the tremor. Tremor slip rates during the deep SSEs also showed two maximum slip patches updip from the region of tremor coinciding with the Kaimanawa (70-80 mm/yr) and Manawatu (~55 mm/yr) SSEs (Figure S5). The maximum tremor slip rate coinciding with the Kaimanawa SSEs was nearly twice as large during SSEs than when not distinguishing times of SSEs. Slip rates in the tremor region were 15-40 mm/yr. The total moment rate was 3.4×10^{19} Nm/yr, while the average moment per tremor burst was 3.0×10^{18} Nm, equivalent to a M_W 5.2.

Results from decomposition of the inter-SSE period were less conclusive due to more stations being less robust. This meant at most stations (9/12 for the east component) the velocity during tremor could not be distinguished from the inter-tremor period with less than a 1σ difference (Figure S10). Since there were still a few stations with at least a 1σ difference, we ran the inversion. Interestingly, the model produced a single slip patch near the tremor source region (max of ~25 mm/yr) and no slip patch in the Manawatu or Kaimanawa SSE regions, albeit there was a poor fit with the model (Figure S7). Slip rates in the tremor region were 5-20 mm/yr. The total moment rate was 9.4×10^{18} Nm/yr, and the average moment per tremor burst was 4.4×10^{17} Nm, equivalent to a M_W 4.6.

4 Small, short-term ETS-like events at deep, central Hikurangi margin

In this study we detected another type of slow slip in this segment of the Hikurangi margin associated with the deep tremor, which we interpret as ETS-like events, a new observation of slow slip for the Hikurangi margin. Our findings support the general idea that seismically observed tectonic tremor can be used to infer the existence of slow slip.

The slip inversion indicated slip on the plate interface in the region of tremor, but maximum slip rates were updip of the tremor and overlapping with the downdip end of the Kaimanawa and Manawatu SSE source regions. This slip was only detectable when tremor occurred during mid- to long-term SSEs, implying that the ETS-like slip associated with tremor is also accompanied by an acceleration of the updip larger SSE. Our data were well-fit with the assumption that slip occurs on the plate interface, but short-term SSEs on structures other than the plate interface cannot be ruled out. While we are confident that the decomposition revealed a geodetic signal associated with the tremor, our ability to interpret the location of slip relative to the tremor was limited. The location of our model was not well-constrained, and there were uncertainties with tremor locations such that we cannot rule out that the tremor and short-term SSEs were indeed co-located. There were a limited number of stations we were able to use up dip of the tremor as those stations included signals from the shallow east coast SSEs. In addition, there were no stations directly on top of the tremor due to the terrain in the region nor were there enough long running stations north of the tremor. Romanet and Ide (2019) noted the relative location of the tremor may not be accurate as they found a standard deviation of 0.15˚ longitude and 0.12˚ latitude for the difference between their locations of earthquakes and the locations given by the GeoNet catalog. Even though the exact location of the deep short-term SSEs relative to the tremor was not fully resolvable at this time, the geodetic signal associated with the tremor was coherent across several stations near the tremor and negligible at far-field stations suggesting that this was a real geodetic signal.

In seeking to characterize the ETS-like events during versus in between the mid- to long-term SSEs, we concluded that short-term ETS-like events could robustly be detected during the mid- to long-term SSEs but those during the inter-SSE periods could not. Decomposition of the inter-SSE time series indicated all but four stations had tremor velocities less than 1σ uncertainty from the mean velocity generated through random decompositions. We suspect this to be a result of too small of a SSE to be detected at all stations even through the decomposition method. However, we speculate that tremor during the inter-SSE periods were occurring with small ETS-like SSEs. Equivalent moment magnitudes of an average tremor burst for each of the three regimes were a good justification for why we can't detect these small short-term ETS-like SSEs individually as they are expected to be below the geodetic detection threshold. However, we demonstrated that decomposition with respect to times of tremor effectively stacks multiple events and served as a method for identification and estimation of size for ETS-like events below the geodetic detection threshold.

To support the fact that the geodetic signal we observed was not simply the mid- to long-term SSE signal, decomposition of the time series during the mid- to long-term SSEs showed displacement rates during tremor were higher than during the SSEs without tremor. Therefore, mid- to long-term SSEs may influence deep short-term SSEs by increasing slip rates for which there are two equivalent interpretations. Under one interpretation, faster slip-rates of ETS-like events during SSEs are driven by the stress shadow effect created by the larger SSEs updip. The SSE that is updip from the tremor will slip faster relatively, generating a stress shadow downdip which will increase the shear stress in the source region of the tremor, hence increasing the rate of tremor failure compared to when mid- to long-term SSEs are not occuring (Frank et al., 2018). The ETS-like slip in turn will add shear stress to the updip SSE region, accelerating ongoing slip there, which may explain our observed tremor-associated slip in the updip SSE regions during the SSE periods (Figure S5). This interpretation is illustrated in Figure 1b. With this understanding, it makes sense that the inter-SSE periods have smaller tremor-associated slip and no slip in the mid- to long-term SSE zones, albeit these results were not robust. Alternatively, we can interpret that the mid- to long-term SSEs merely fluctuate and move in and out of the tremor-generating region, generating tremor only when they enter this region, which tends to be when the slip rate is higher in the adjacent updip region. These interpretations can be seen as essentially equivalent during the mid- to long-term SSEs. However, we interpret the occurrence of tremor outside the times of mid- to long-term SSEs as evidence for the first interpretation.

5 Conclusions

This study identified and modeled a geodetic signal associated with deep tectonic tremor. We found the plate interface below the deep mid- to long-term SSEs in Manawatu and Kaimanawa regions may slip often, in small, short-term SSEs with tremor, which we refer to as ETS-like (Figure 1b). This is a new observation of slow slip behavior in New Zealand which implies that there are three types of slow slip that overlap along-strike, 1) shallow, short-term SSEs, 2) deep, mid- to long-term SSEs, and 3) deeper, short-term ETS-like SSEs with tremor. In addition, the mid- to long-term SSEs may influence the deep, short-term ETS-like events by increasing slip rates, and the ETS-like events in turn may increase slip rates in mid-to-long term SSEs. Similar observations of deep, small, short-term SSEs co-located with tremor and long-term SSEs located updip from tremor have been observed in Japan, Mexico and Alaska (Frank et al., 2018; Hirose & Obara, 2005; Hirose et al., 2010; Rousset et al., 2019). However, the Hikurangi margin also has shallow, short-term SSEs which may be separated from the region of mid- to long-term SSEs by a region of creeping (Wallace, 2020). The nature of the strong variabilities in SSE depths and durations in the central Hikurangi margin is still not well understood.

The decomposition method relies on a catalog of tremor to ensure proper identification of start and end times of tremor bursts which are subsequently used for measuring displacement increments and tremor-associated velocities. Tremor is difficult to detect in New Zealand as the high rates of seismicity make automatic detection and location of tremor challenging, and we expect that the tremor catalog is incomplete (Romanet & Ide, 2019). We do not know if tremor bursts were missed or if apparent durations are a mis-representation of the true duration due to too few events able to be detected. Therefore, the tremor catalog is one caveat to this method and results from this study are meant to be an estimation of average tremor velocities and slip rates. As network coverage, tremor detection methods, and detection of low-frequency earthquakes improve in New Zealand, the spatiotemporal relationship between deep, ETS-like events and mid- to long-term SSEs can be better understood.

Acknowledgments

This work was supported by departmental funds from the University of Kansas Geology Department. The authors thank Dr. Laura Wallace for her insightful discussions which benefited this study. The authors also thank graphic designer Hailey Stepanek for helping make Figure 1b.

Data Availability Statement

Daily time-series solutions from continuous GNSS stations can be obtained from the GeoNet Aotearoa New Zealand Continuous GNSS Network (https://doi.org/10.21420/30F4-1A55).

Timing of the offsets were obtained from the University of Nevada-Reno steps database (http://geodesy.unr.edu/NGLStationPages/steps.txt). The tectonic tremor catalog from Romanet and Ide (2019) is available via https://doi.org/10.1186/s40623-019-1039-1

References

Aagaard, B. T., Knepley, M. G., & Williams, C. A. (2013). A domain decomposition approach to implementing fault slip in finite-element models of quasi-static and dynamic crustal deformation. *Journal of Geophysical Research Solid Earth*, 118, 3059–3079. https://doi.org/10.1002/jgrb.50217

Aagaard, B. T., Knepley, M. G., & Williams, C. A. (2017a). PyLith v2.2.1, Computational Infrastructure for Geodynamics. https://doi.org/10.5281/zenodo.886600, Retrieved from https://geodynamics.org/cig/software/pylith/

Aagaard, B. T., Knepley, M. G., & Williams, C. A. (2017b). PyLith user manual, version 2.2.0, Computational Infrastructure for Geodynamics, Davis, CA. Retrieved from https://geodynamics.org/cig/software/github/pylith/v2.2.0/pylith-2.2.0_manual.pdf

Altamimi, Z., Métivier, L., & Collilieux, X. (2012). ITRF2008 plate motion model. *Journal of Geophysical Research: Solid Earth*, *117*(B7). https://doi.org/10.1029/2011JB008930

Bartlow, N. M. (2020). A long-term view of episodic tremor and slip in Cascadia. *Geophysical Research Letters*, *47*(3), e2019GL085303. https://doi.org/10.1029/2019GL085303

Bartlow, N. M., Miyazaki, S. I., Bradley, A. M., & Segall, P. (2011). Space-time correlation of slip and tremor during the 2009 Cascadia slow slip event. *Geophysical Research Letters*, *38*(18). https://doi.org/10.1029/2011GL048714

Bartlow, N. M., Wallace, L. M., Beavan, R. J., Bannister, S., & Segall, P. (2014). Time-dependent modeling of slow slip events and associated seismicity and tremor at the Hikurangi subduction zone, New Zealand. *Journal of Geophysical Research: Solid Earth*, *119*(1), 734–753. https://doi.org/10.1002/2013JB010609

Beavan, J., Tregoning, P., Bevis, M., Kato, T., & Meertens, C. (2002). Motion and rigidity of the Pacific Plate and implications for plate boundary deformation. *Journal of Geophysical Research: Solid Earth*, *107*(B10), ETG-19. https://doi.org/10.1029/2001JB000282

Beroza, G. C., & Ide, S. (2011). Slow earthquakes and nonvolcanic tremor. *Annual review of Earth and planetary sciences*, *39*, 271–296. https://doi.org/10.1146/annurev-earth-040809-152531

Brown, J. R., Beroza, G. C., Ide, S., Ohta, K., Shelly, D. R., Schwartz, S. Y., et al. (2009). Deep low-frequency earthquakes in tremor localize to the plate interface in multiple subduction zones. *Geophysical Research Letters*, *36*(19). https://doi.org/10.1029/2009GL040027

Delahaye, E. J., Townend, J., Reyners, M. E., & Rogers, G. (2009). Microseismicity but no tremor accompanying slow slip in the Hikurangi subduction zone, New Zealand. *Earth and Planetary Science Letters*, *277*(1-2), 21–28. https://doi.org/10.1016/j.epsl.2008.09.038

Dragert, H., Wang, K., & James, T. S. (2001). A silent slip event on the deeper Cascadia subduction interface. *Science*, *292*(5521), 1525–1528. https://doi.org/10.1126/science.1060152

Eberhart-Phillips, D., & Bannister, S. (2015). 3-D imaging of the northern Hikurangi subduction zone, New Zealand: Variations in subducted sediment, slab fluids and slow slip. *Geophysical Journal International*, *201*(2), 838–855. https://doi.org/10.1093/gji/ggv057

Eberhart-Phillips, D., & Reyners, M. (2012). Imaging the Hikurangi plate interface region with improved local-earthquake tomography. *Geophysical Journal International*, *190*(2), 1221–1242. https://doi.org/10.1111/j.1365-246X.2012.05553.x

Eberhart-Phillips, D., Reyners, M., Bannister, S., Chadwick, M., & Ellis, S. (2010). Establishing a versatile 3-D seismic velocity model for New Zealand. *Seismological Research Letters*, *81*(6), 992–1000. https://doi.org/10.1785/gssrl.81.6.992

Frank, W. B., Rousset, B., Lasserre, C., & Campillo, M. (2018). Revealing the cluster of slow transients behind a large slow slip event. *Science advances*, *4*(5), eaat0661. https://doi.org/10.1126/sciadv.aat0661

Gao, X., & Wang, K. (2017). Rheological separation of the megathrust seismogenic zone and episodic tremor and slip. *Nature*, *543*(7645), 416–419. https://doi.org/10.1038/nature21389

GNS Science. (2000). GeoNet Aotearoa New Zealand Continuous GNSS Network Time Series Dataset [Data set]. GNS Science, GeoNet. https://doi.org/10.21420/30F4-1A55

Graham, S. E., DeMets, C., Cabral-Cano, E., Kostoglodov, V., Walpersdorf, A., Cotte, N., et al., (2014). GPS constraints on the 2011–2012 Oaxaca slow slip event that preceded the 2012

March 20 Ometepec earthquake, southern Mexico. *Geophysical Journal International*, *197*(3), 1593–1607. https://doi.org/10.1093/gji/ggu019

Hawthorne, J. C., & Rubin, A. M. (2013). Short-time scale correlation between slow slip and tremor in Cascadia. *Journal of Geophysical Research: Solid Earth*, *118*(3), 1316–1329. https://doi.org/10.1002/jgrb.50103

Hirose, H., Y. Asano, K. Obara, T. Kimura, T. Matsuzawa, S. Tanaka, and T. Maeda (2010). Slow earthquakes linked along dip in the Nankai subduction zone. *Science*, *330*, 1502. https://doi.org/10.1126/science.1197102

Hirose, H., & Obara, K. (2005). Repeating short-and long-term slow slip events with deep tremor activity around the Bungo channel region, southwest Japan. *Earth, planets and space*, *57*(10), 961–972. https://doi.org/10.1186/BF03351875

Hyndman, R. D., McCrory, P. A., Wech, A., Kao, H., & Ague, J. (2015). Cascadia subducting plate fluids channelled to fore-arc mantle corner: ETS and silica deposition. *Journal of Geophysical Research: Solid Earth*, *120*(6), 4344–4358. https://doi.org/10.1002/2015JB011920

Ide, S., Shelly, D. R., & Beroza, G. C. (2007). Mechanism of deep low frequency earthquakes: Further evidence that deep non-volcanic tremor is generated by shear slip on the plate interface. *Geophysical Research Letters*, *34*(3). https://doi.org/10.1029/2006GL028890

Jacobs, K. M., Savage, M. K., & Smith, E. C. G. (2016). Quantifying seismicity associated with slow slip events in the Hikurangi margin, New Zealand. *New Zealand Journal of Geology and Geophysics*, *59*(1), 58–69. https://doi.org/10.1080/00288306.2015.1127827

Kato, A., Obara, K., Igarashi, T., Tsuruoka, H., Nakagawa, S., & Hirata, N. (2012). Propagation of slow slip leading up to the 2011 Mw 9.0 Tohoku-Oki earthquake. *Science*, *335*(6069), 705–708. https://doi.org/10.1126/science.1215141.

Langridge, R. M., Ries, W. F., Litchfield, N. J., Villamor, P., Van Dissen, R. J., Barrell, D. J. A., et al., (2016). The New Zealand Active Faults Database. *New Zealand Journal of Geology and Geophysics*, *59*, 86–96. https://doi.org/0.1080/00288306.2015.1112818

Obara, K. (2002). Nonvolcanic deep tremor associated with subduction in southwest Japan. *Science*, *296*(5573), 1679–1681. https://doi.org/10.1126/science.1070378

Obara, K., Hirose, H., Yamamizu, F., & Kasahara, K. (2004). Episodic slow slip events accompanied by non-volcanic tremors in southwest Japan subduction zone. *Geophysical Research Letters*, *31*(23). https://doi.org/10.1029/2004GL020848

Obara, K., & Kato, A. (2016). Connecting slow earthquakes to huge earthquakes. *Science*, *353*(6296), 253–257. https://doi.org/10.1126/science.aaf1512

Radiguet, M., Cotton, F., Vergnolle, M., Campillo, M., Walpersdorf, A., Cotte, N., & Kostoglodov, V. (2012). Slow slip events and strain accumulation in the Guerrero gap, Mexico. *Journal of Geophysical Research: Solid Earth*, *117*(B4). https://doi.org/10.1029/2011JB008801

Radiguet, M., Perfettini, H., Cotte, N., Gualandi, A., Valette, B., Kostoglodov, V., et al. (2016). Triggering of the 2014 M w 7.3 Papanoa earthquake by a slow slip event in Guerrero, Mexico. *Nature Geoscience*, *9*(11), 829–833. https://doi.org/10.1038/ngeo2817

Reyners, M., & Bannister, S. (2007). Earthquakes triggered by slow slip at the plate interface in the Hikurangi subduction zone, New Zealand. *Geophysical research letters*, *34*(14). https://doi.org/10.1029/2007GL030511

Reyners, M., Eberhart-Phillips, D., & Martin, S. (2014). Prolonged Canterbury earthquake sequence linked to widespread weakening of strong crust. *Nature Geoscience*, *7*(1), 34–37. https://doi.org/10.1038/ngeo2013

Rogers, G., & Dragert, H. (2003). Episodic tremor and slip on the Cascadia subduction zone: The chatter of silent slip. *Science*, *300*(5627), 1942–1943. https://doi.org/10.1126/science.1084783

Romanet, P., & Ide, S. (2019). Ambient tectonic tremors in manawatu, Cape Turnagain, marlborough, and Puysegur, New Zealand. *Earth, Planets and Space*, *71*(1), 1–9. https://doi.org/10.1186/s40623-019-1039-1

Rousset, B., Fu, Y., Bartlow, N., & Bürgmann, R. (2019). Weeks-long and years-long slow slip and tectonic tremor episodes on the south central Alaska Megathrust. *Journal of Geophysical Research: Solid Earth*, *124*(12), 13392–13403. https://doi.org/10.1029/2019JB018724

Ruiz, S., Metois, M., Fuenzalida, A., Ruiz, J., Leyton, F., Grandin, R., et al., (2014). Intense foreshocks and a slow slip event preceded the 2014 Iquique M w 8.1 earthquake. *Science*, *345*(6201), 1165–1169. https://doi.ord/10.1126/science.1256074

Shaddox, H. R., & Schwartz, S. Y. (2019). Subducted seamount diverts shallow slow slip to the forearc of the northern Hikurangi subduction zone, New Zealand. *Geology*, *47*(5), 415–418. https://doi.org/10.1130/G45810.1

Shelly, D. R., Beroza, G. C., & Ide, S. (2007). Non-volcanic tremor and low-frequency earthquake swarms. *Nature*, *446*(7133), 305–307. https://doi.org/10.1038/nature05666

Shelly, D. R., Beroza, G. C., Ide, S., & Nakamula, S. (2006). Low-frequency earthquakes in Shikoku, Japan, and their relationship to episodic tremor and slip. *Nature*, *442*(7099), 188–191. https://doi.org/10.1038/nature04931

Todd, E. K., & Schwartz, S. Y. (2016). Tectonic tremor along the northern Hikurangi Margin, New Zealand, between 2010 and 2015. *Journal of Geophysical Research: Solid Earth*, *121*(12), 8706–8719. https://doi.org/10.1002/2016JB013480

Todd, E. K., Schwartz, S. Y., Mochizuki, K., Wallace, L. M., Sheehan, A. F., Webb, S. C., et al. (2018). Earthquakes and tremor linked to seamount subduction during shallow slow slip at the Hikurangi margin, New Zealand. *Journal of Geophysical Research: Solid Earth*, *123*(8), 6769–6783. https://doi.org/10.1029/2018JB016136

Villafuerte, C., & Cruz-Atienza, V. M. (2017). Insights into the causal relationship between slow slip and tectonic tremor in Guerrero, Mexico. *Journal of Geophysical Research: Solid Earth*, *122*(8), 6642–6656. https://doi.org/10.1002/2017JB014037

Wallace, L. M. (2020). Slow slip events in New Zealand. *Annual Review of Earth and Planetary Sciences*, *48*, 175–203. https://doi.org/10.1146/annurev-earth-071719-055104

Wallace, L. M., Barnes, P., Beavan, J., Van Dissen, R., Litchfield, N., Mountjoy, J., et al. (2012). The kinematics of a transition from subduction to strike-slip: An example from the central New Zealand plate boundary. *Journal of Geophysical Research: Solid Earth*, *117*(B2). https://doi.org/10.1029/2011JB008640

Wallace, L. M., & Beavan, J. (2010). Diverse slow slip behavior at the Hikurangi subduction margin, New Zealand. *Journal of Geophysical Research: Solid Earth*, *115*(B12). https://doi.org/10.1029/2010JB007717

Wallace, L. M., Beavan, J., Bannister, S., & Williams, C. (2012). Simultaneous long-term and short-term slow slip events at the Hikurangi subduction margin, New Zealand: Implications for processes that control slow slip event occurrence, duration, and migration. *Journal of Geophysical Research: Solid Earth*, *117*(B11). https://doi.org/10.1029/2012JB009489

Wallace, L. M., & Eberhart-Phillips, D. (2013). Newly observed, deep slow slip events at the central Hikurangi margin, New Zealand: Implications for downdip variability of slow slip and tremor, and relationship to seismic structure. *Geophysical Research Letters*, *40*(20), 5393–5398. https://doi.org/10.1002/2013GL057682

Wech, A. G., & Creager, K. C. (2007). Cascadia tremor polarization evidence for plate interface slip. *Geophysical Research Letters*, *34*(22). https://doi.org/10.1029/2007GL031167

Williams, C. A., Eberhart-Phillips, D., Bannister, S., Barker, D. H. N., Henrys, S., Reyners, M., & Sutherland, R. (2013). Revised interface geometry for the Hikurangi subduction zone, New Zealand. *Seismological Research Letters*, *84*(6), 1066–1073. https://doi.org/10.1785/0220130035

Williams, C. A., & Wallace, L. M. (2015). Effects of material property variations on slip estimates for subduction interface slow-slip events. *Geophysical Research Letters*, *42*(4), 1113–1121. https://doi.org/10.1002/2014GL062505

Williams, C. A., & Wallace, L. M. (2018). The impact of realistic elastic properties on inversions of shallow subduction interface slow slip events using seafloor geodetic data. *Geophysical Research Letters*, *45*, 7462–7470. https://doi.org/10.1029/2018GL078042

Wu, Z. L., & Chen, Y. T. (2003). Definition of seismic moment at a discontinuity interface. *Bulletin of the Seismological Society of America*, 93(4), 1832–1834. https://doi.org/10.1785/0120020234

Yabe, S., Ide, S., & Yoshioka, S. (2014). Along-strike variations in temperature and tectonic tremor activity along the Hikurangi subduction zone, New Zealand. *Earth, Planets and Space*, *66*, 1–15. https://doi.org/10.1186/s40623-014-0142-6

Yarce, J., Sheehan, A. F., Nakai, J. S., Schwartz, S. Y., Mochizuki, K., Savage, M. K., et al. (2019). Seismicity at the northern Hikurangi Margin, New Zealand, and investigation of the potential spatial and temporal relationships with a shallow slow slip event. *Journal of Geophysical Research: Solid Earth*, *124*(5), 4751–4766. https://doi.org/10.1029/2018JB017211

AGU PUBLICATIONS

Geophysical Research Letters

Supporting Information for

Deep Short-term Slow Slip and Tremor in the Manawatu Region, New Zealand

Shannon L. Fasola[1], Noel M. Jackson[1], and Charles A. Williams[2]

[1]Department of Geology, University of Kansas, Lawrence, KS.

[2]GNS Science, Lower Hutt, New Zealand.

Contents of this file

Introduction

This Supporting Information includes details on the methods used and additional figures supporting the main text.

Text S1. Methods

GNSS Post-Processing

For this study we used daily time-series solutions from continuous GNSS stations from the GeoNet network on the North Island (GNS Science, 2000). GNSS data processing methods are outlined on the GeoNet website. We referenced GNSS time series to the fixed Australian plate using the plate model of Altamimi et al. (2012). Offsets due to antenna changes and earthquakes were estimated by differencing the average positions of 10 days before and after the offset and were then removed. Timing of the offsets were obtained from the University of Nevada-Reno steps database (http://geodesy.unr.edu/NGLStationPages/steps.txt). Outliers, any day for which there was more than a 4 mm difference in the horizontal position and/or more than a 14 mm difference in the vertical position from a running mean with a window of 6 data points, were removed from all 3 components regardless of which criteria was met. There was a common mode signal on all stations in the network. Therefore, we regionally filtered the time series by averaging a select set of detrended time series with offsets removed from stations far from the Hikurangi Trench that have close to linear behavior. Regional stations used for averaging were AUCK, CORM, KTIA, WARK, WHNG (Figure S1). The averaged time series (i.e., the common mode signal) was then subtracted from the stations that exhibit tectonic deformation.

Determining Surface Velocity Uncertainties

The uncertainty of the inter-tremor velocities ($\sigma_{inter\text{-}tremor}$) for each of the three scenarios was determined by taking the standard deviation from a population of velocities generated through random resampling of the displacement increments. For each set, we randomly resampled the displacement increments without replacement 10,000 times, generated a cumulative displacement time series and performed a linear regression on the cumulative displacement time series to obtain a velocity for each iteration. We kept the duration of the displacement increment during resampling. Since the true tremor velocity was calculated by subtracting the inter-tremor velocity from the uncorrected tremor velocity, we similarly found the uncertainty of the uncorrected tremor velocity ($\sigma_{tremor\ before\ correction}$) through random resampling and then propagated uncertainties to determine the uncertainty of the true tremor velocity (σ_{tremor}):

$$\sigma_{tremor} = \sqrt{(\sigma_{\ tremor\ before\ correction})^2 + (\sigma_{\ inter-tremor})^2}$$

Robustness of Decompositions

In order to quantify the robustness of these decompositions with regard to background noise levels, we followed the modified bootstrapping approach of Rousset et al. (2019). Using the same number of tremor clusters as in the catalog, we randomly chose start times from the time series and randomly sampled the tremor durations without replacement to generate a synthetic catalog of tremor clusters to perform decompositions with. Periods of tremor from the real catalog were removed before running the decompositions with the synthetic tremor catalog. For decomposition of the SSE and inter-SSE times, we also removed periods of inter-SSE and SSE, respectively, to generate a synthetic 'SSE-only time series' and 'inter-SSE-only time series'. We performed these decompositions for 1) the entire time series, 2) during mid-to-long-term SSE time series, and 3) inter-SSE time series for the horizontal components 10,000 times and assumed that the decomposition was robust if the average velocity acquired for the real tremor periods was more than 2σ from the mean of velocities obtained with the random decompositions associated with noise or the inter-tremor periods. Rousset et al. (2019) used a 3σ threshold, but due to the likely incomplete tremor catalog, we lowered the threshold to 2σ. The decompositions for the entire time series were found to be robust for the east component of eight stations (Figure S7). The decompositions for the SSE time series were also found to be robust for the east component of eight stations (Figure S8). Fewer stations were found to be robust for the north components, mainly because they are less sensitive to slip on the subduction interface. The random decompositions for the inter-SSE time series indicated a smaller difference between the real average velocity of tremor periods and the mean of the randomly generated velocities. For the east and north components no stations were greater than 2σ but 3 and 4 were greater than 1σ, respectively (Figure S9).

This modified bootstrapping technique as a method of testing the robustness of the decompositions is station specific. Therefore, we ran the decomposition on a select number of GNSS stations on the southern part of the North Island which was further from the Manawatu tremor, other regions of SSEs, and the Taupo volcanic zone to confirm that the tremor associated signal was confined to where tremor was observed (Figure 3b). To further support the validity of a geodetic signal only at stations nearest the tremor, we applied the modified bootstrapping technique to those far-field stations on which we ran the decompositions. As we expected, none of the east component time-averaged velocities of the far-field stations were found to be robust for decomposition of the entire time series, signifying the decomposition method of the Manawatu tremor did not detect a discernible geodetic signal at stations further from the tremor.

Calculation of Moment Rates

We calculated a total moment rate for each of the three modeled slip rate solutions. For each triangular patch, we found the time-averaged moment rate using the slip rate, area, and effective shear modulus for that patch and then summed the moment rates for the entire slip area. We consider both the variation of the shear modulus within the volume as well as possible 'jumps' in the shear modulus across the fault. To do this, we sample the properties on either side of the fault, assuming a distance of 100 m normal to the fault on each side, and then compute an effective shear modulus using the technique described by Wu and Chen (2003). We estimated the average moment per tremor burst by multiplying the moment rate for each slip patch by the average duration of tremor burst for that regime and totaling the moment (Table S1).

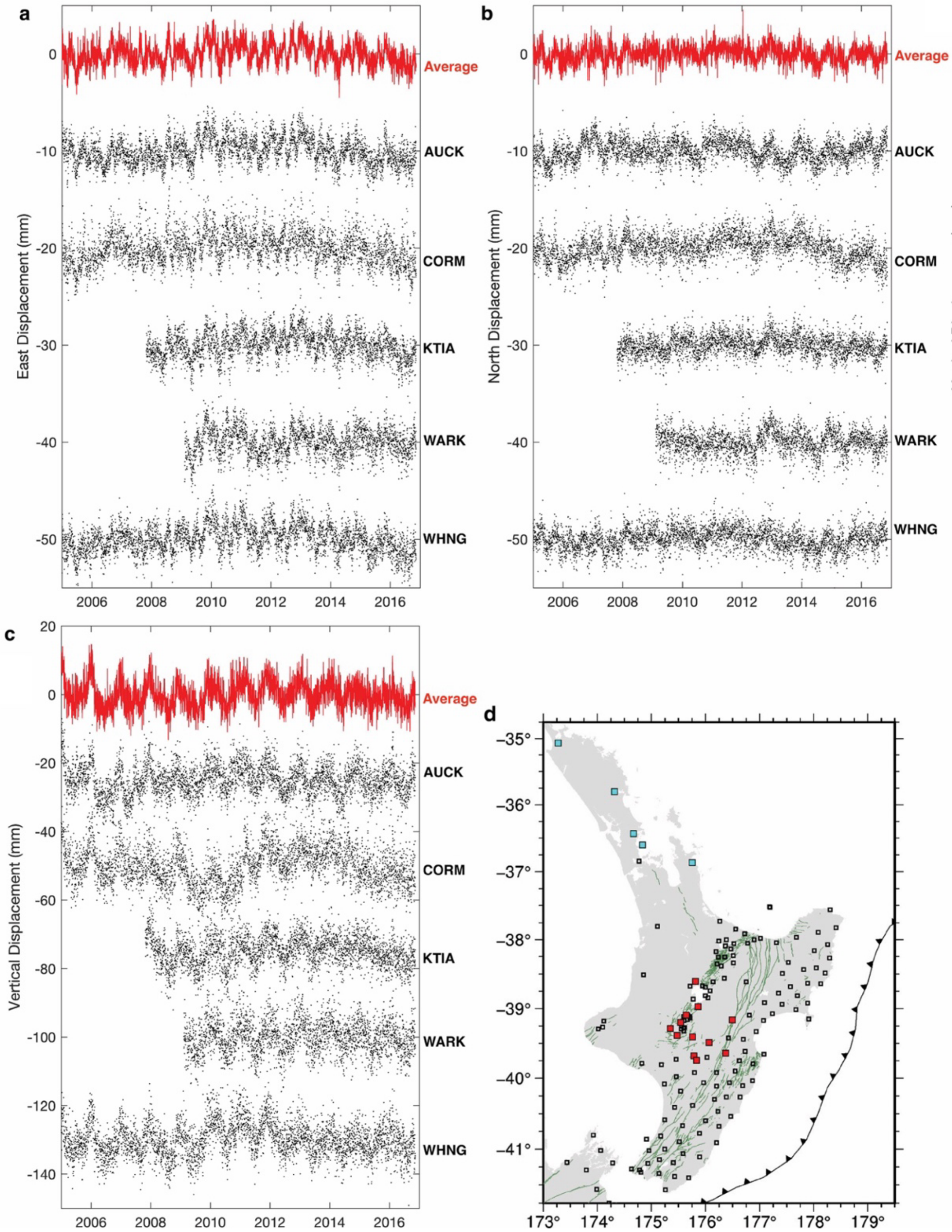

Figure S1. Time series of regional common mode signal. Black dots are detrended GNSS time series with offsets removed from stations far from the Hikurangi Trench that have close to linear behavior and were used in averaging to determine the common mode signal. Red line represents the average of those regional time series. a) East component. b) North component. c) Vertical component. d) Map of GeoNet GNSS stations (squares). Stations used for determining common mode signal and for decomposition are colored light blue and red, respectively.

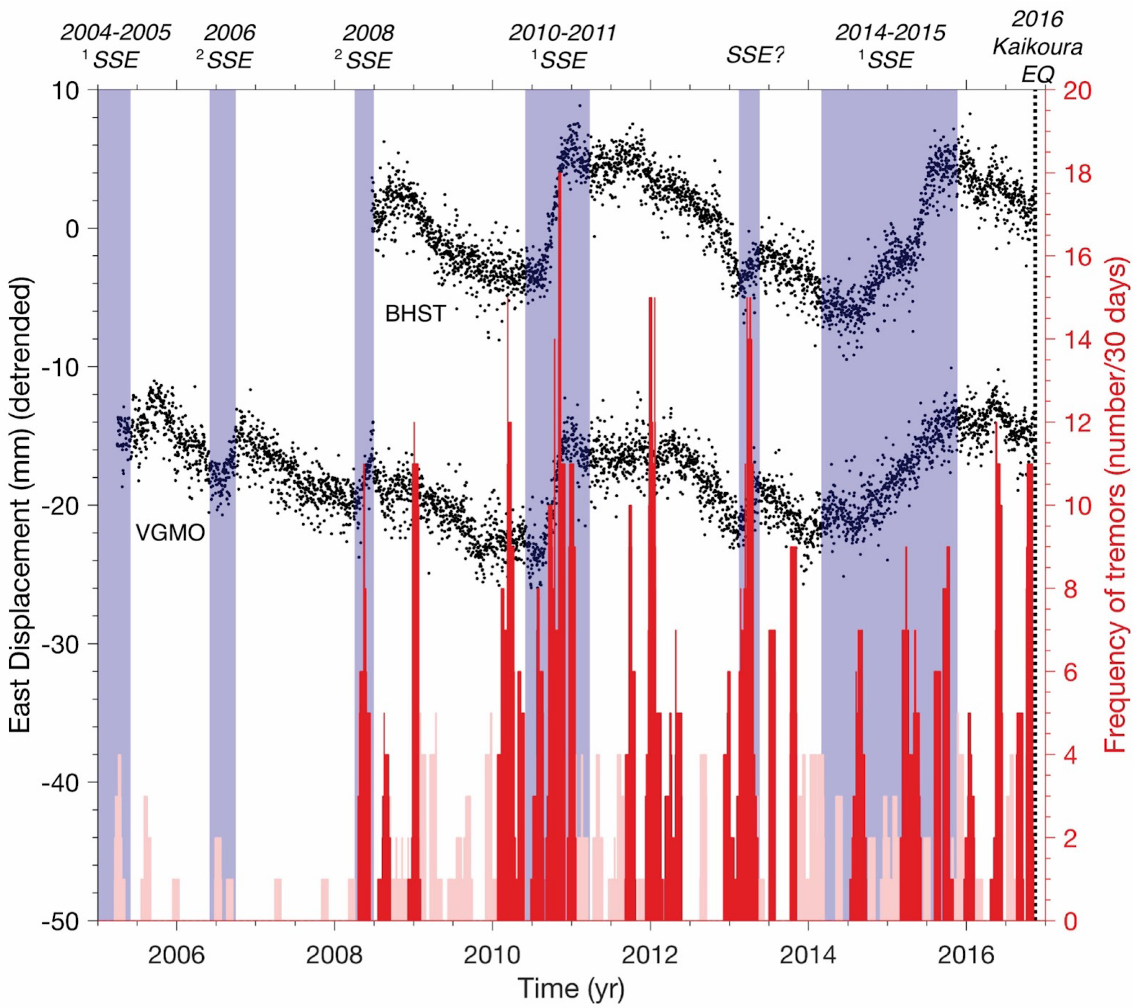

Figure S2. Tremor density and GNSS displacement plot. The tremor density (red and pink bars) is based on a 30-day moving window of the tremor catalog from Romanet and Ide (2019). Red bars are tremor that met the criteria to be in a cluster using a minimum of 5 events per cluster and a minimum inter-cluster duration of 22 days. The GNSS displacements consist of the detrended daily eastward displacements (black dots) at the BHST and VGMO GeoNet GNSS stations. Purple shaded areas represent timing of known deep mid- to long-term SSEs in the [1]Manawatu and [2]Kaimanawa regions, respectively. There may have been a deep SSE in 2013 similar to the 2006 and 2008 mid-term Kaimanawa SSEs (personal communication with Laura Wallace) which is also shaded purple. Black dotted line marks the time of the 2016 M_W 7.8 Kaikoura earthquake and the end of data analyzed in this study.

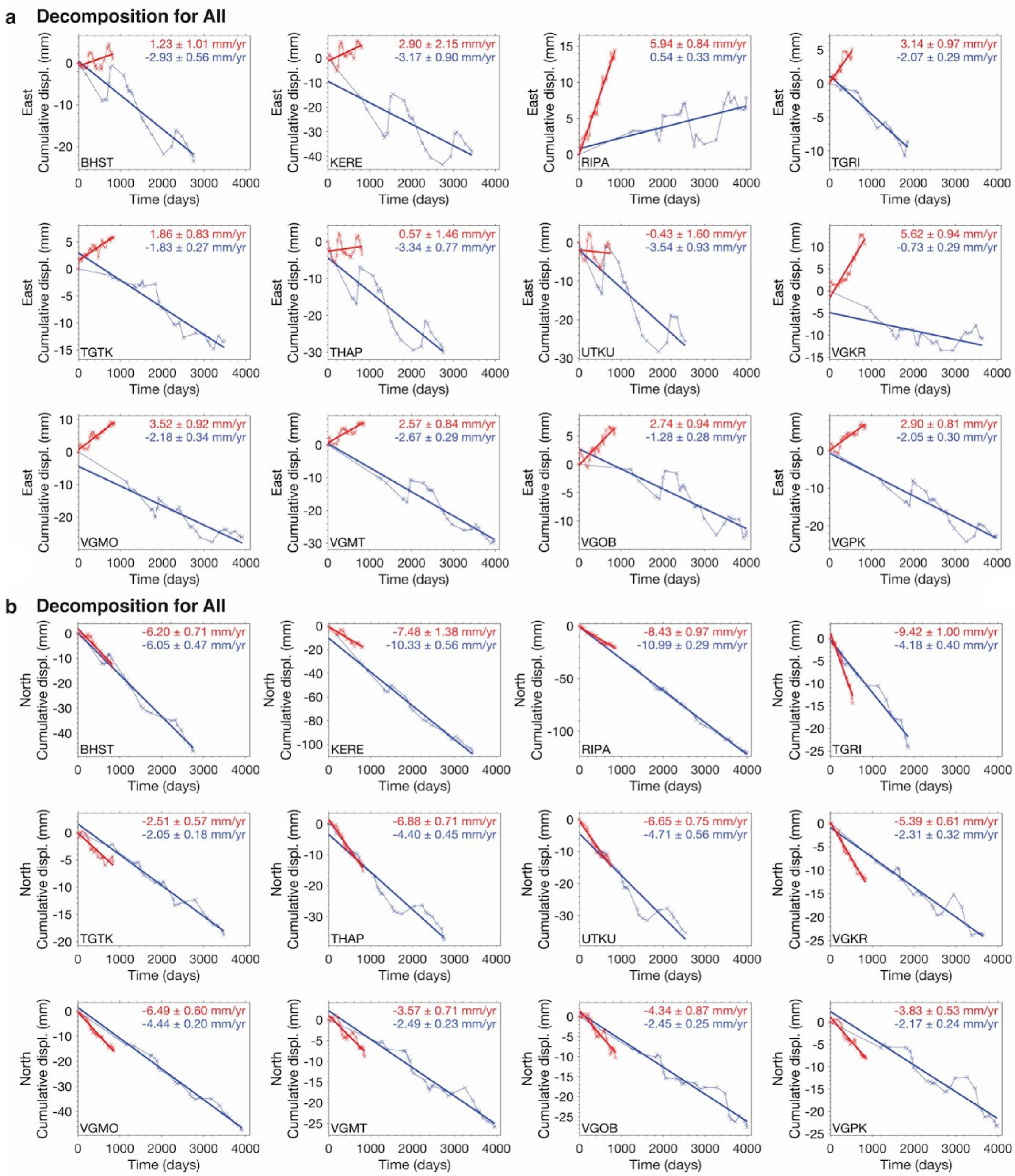

Figure S3. Decomposition of the entire time series a) east and b) north components from 2005 until the 2016 Kaikoura earthquake. Red and blue curves indicate cumulative offsets during tremor and inter-tremor periods, respectively. Values represent slope of the best fit line and 1σ uncertainty determined from random resampling of cumulative displacement increments.

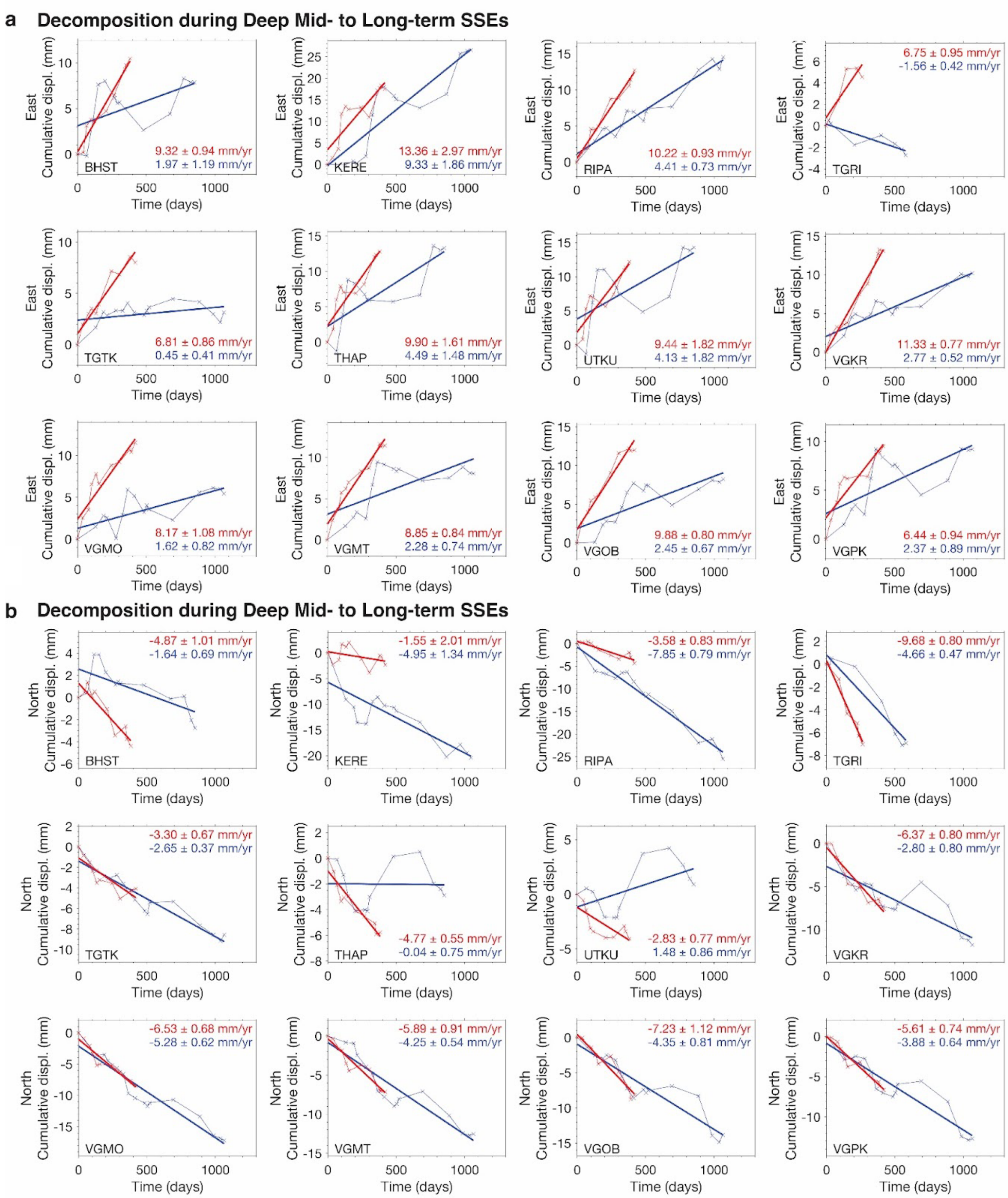

Figure S4. Decomposition of the GNSS time series a) east and b) north components during known deep 2004-2005, 2006, 2008, 2010-2011, 2013, and 2014-2015 slow slip events in the Manawatu and Kaimanawa regions. Red and blue curves indicate cumulative offsets during tremor and inter-tremor periods, respectively. Values represent slope of the best fit line and 1σ uncertainty determined from random resampling of cumulative displacement increments.

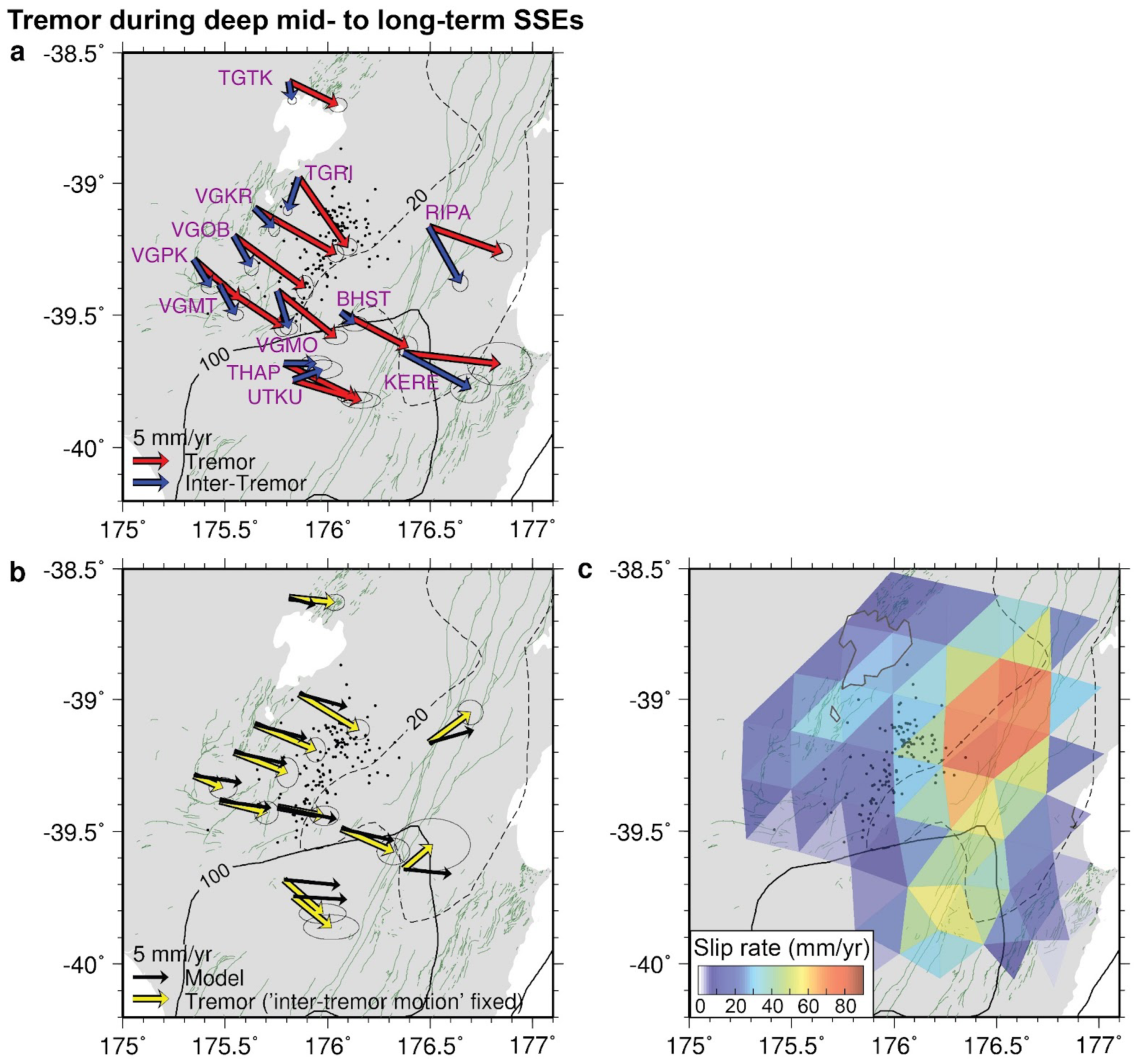

Figure S5. Time-averaged displacement rate and slip rate for tremor bursts during the mid- to long-term SSEs in Manawatu and Kaimanawa regions. a) Displacement rate of tremor (red arrows) and inter-tremor periods (blue arrows) with 1σ uncertainties are shown. b) Comparison of the true tremor displacement rates with the 'inter-tremor motion' fixed (yellow arrows) and 1σ uncertainty and modeled tremor displacement rates obtained from inversion (black arrows). c) Time-averaged slip rate during tremor bursts as estimated by static slip inversion.

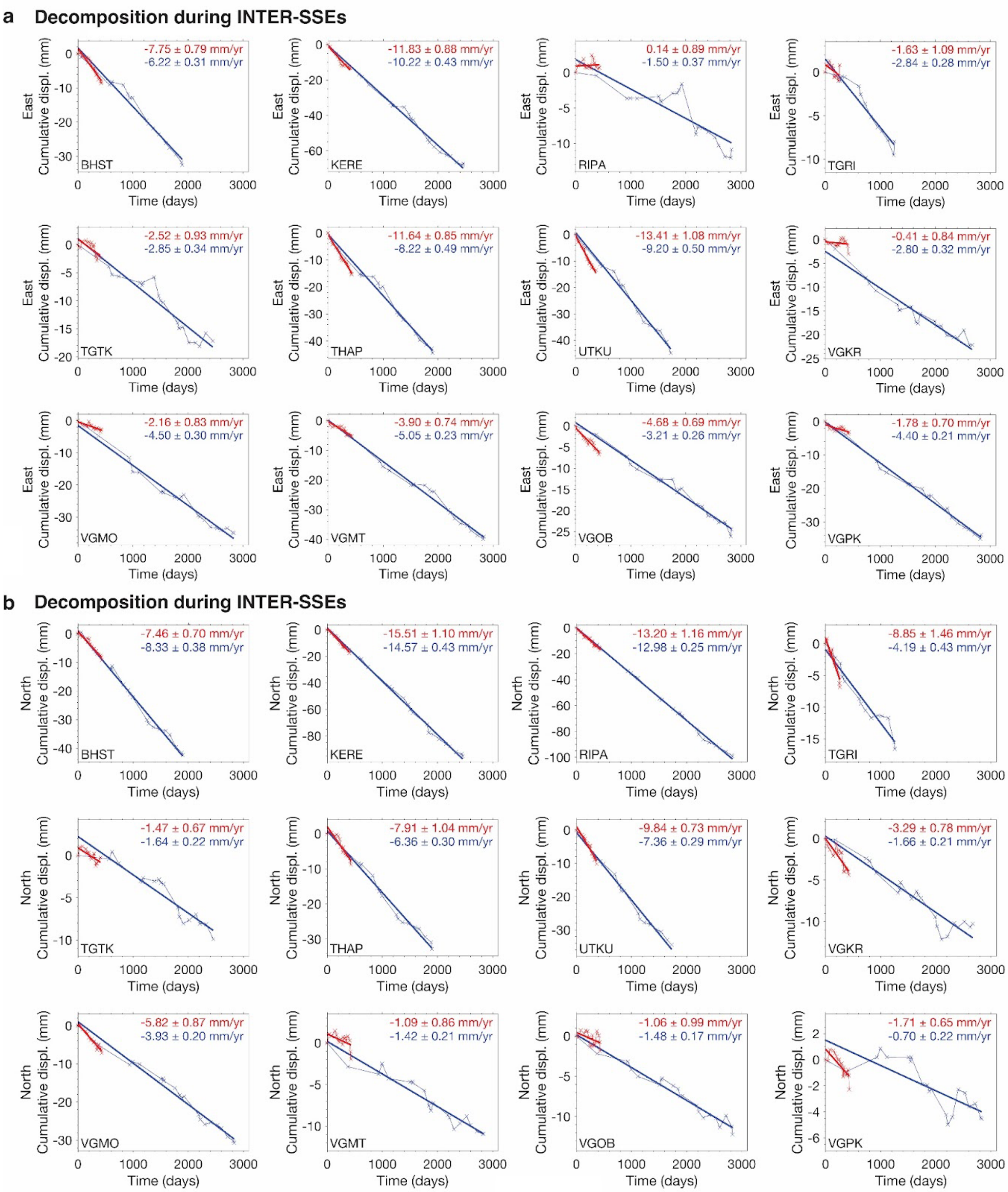

Figure S6. Decomposition of the GNSS time series. a) east and b) north components during inter-SSE time in the Manawatu and Kaimanawa regions: 2005 SSE to 2006 SSE, 2006 SSE to 2008 SSE, 2008 SSE to 2010-2011, 2010-2011 SSE to 2013 SSE, 2013 SSE to 2014-2015 SSE, and 2014-2015 to 2016 Kaikoura earthquake. The red and blue curves indicate the cumulative offsets during tremor and inter-tremor periods, respectively. Values represent slope of the best fit line and 1σ uncertainty determined from random resampling of cumulative displacement increments.

Tremor during INTER-SSEs

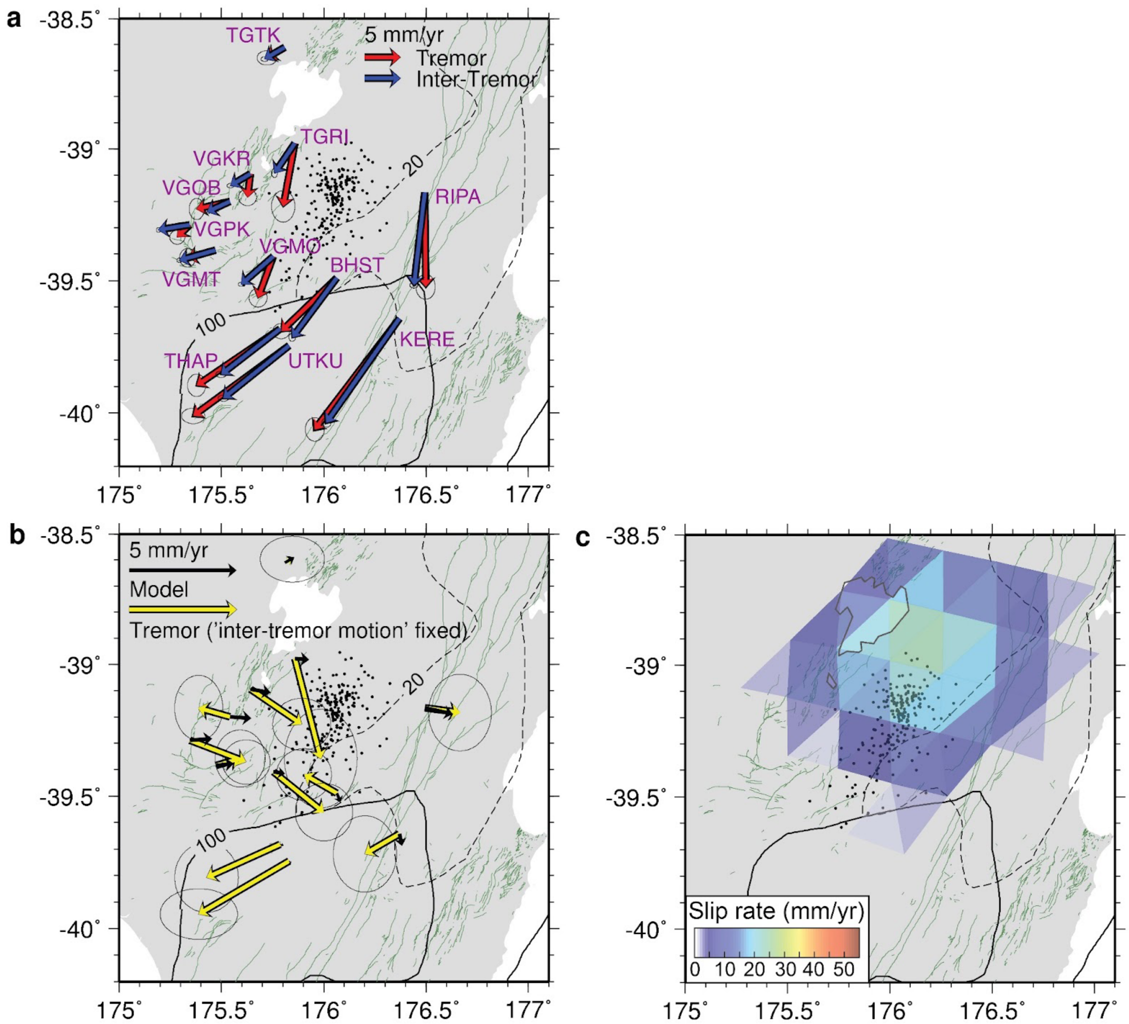

Figure S7. Time-averaged displacement rate and slip rate for tremor bursts during the inter-SSE periods. a) Displacement rate of tremor (red arrows) and inter-tremor periods (blue arrows) with 1σ uncertainties are shown. b) Comparison of the true tremor displacement rates with the 'inter-tremor motion' fixed (yellow arrows) and 1σ uncertainty and modeled tremor displacement rates obtained from inversion (black arrows). Due to the small values of the modeled vectors, we enlarged the 5 mm/yr scale. c) Time-averaged slip rate during tremor bursts as estimated by static slip inversion.

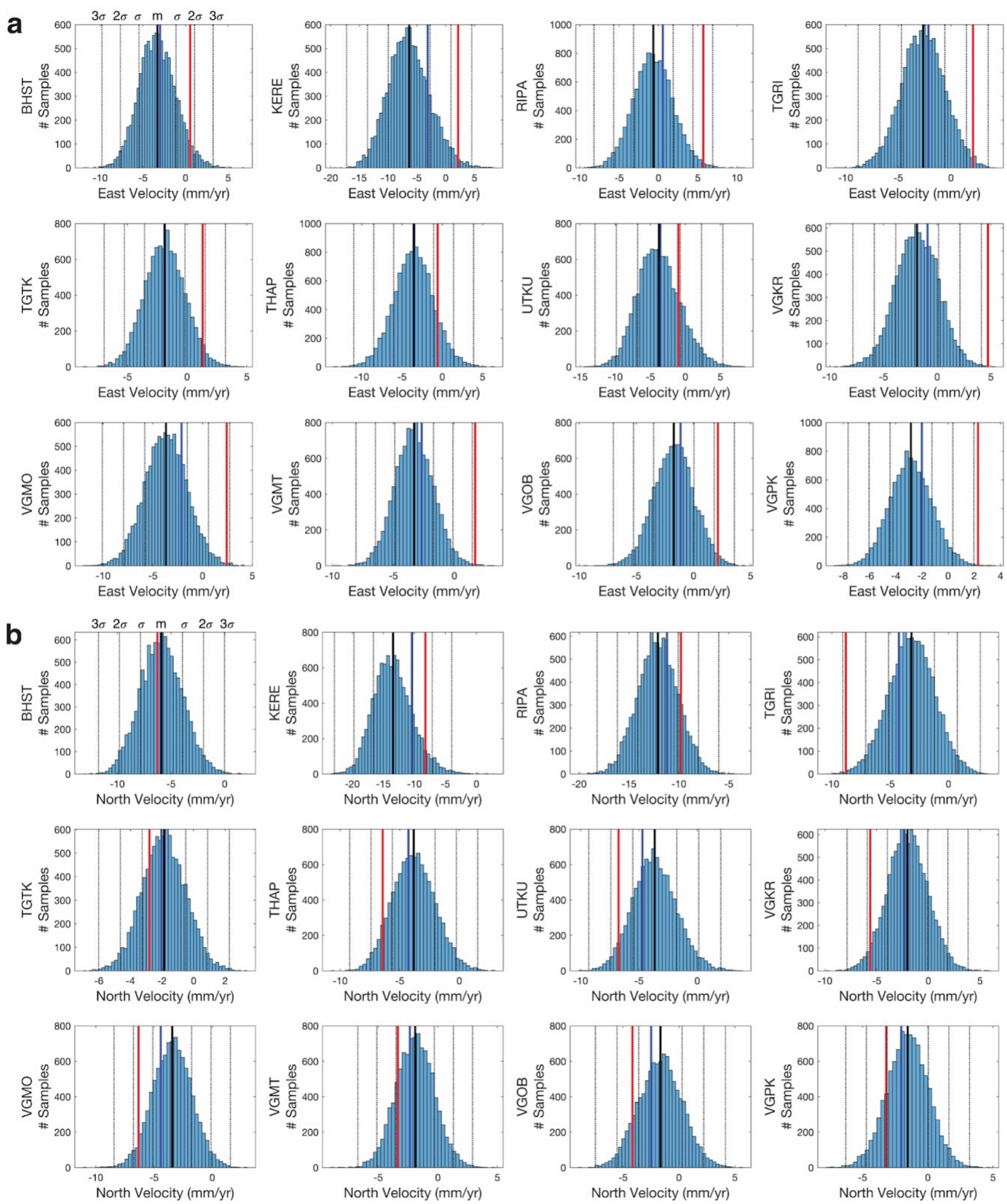

Figure S8. Histogram of velocities obtained by random decomposition of the entire time series with known tremor periods removed. For the decomposition, we randomly selected times of tremor clusters with the same number of clusters and durations as the real tremor catalog. The mean of the distribution is indicated by a solid black line whereas the σ, 2σ, and 3σ of the distribution are indicated by dashed lines. The red and blue lines indicate the averaged velocities obtained respectively for the tremor and inter-tremor periods. a) East velocity. b) North velocity.

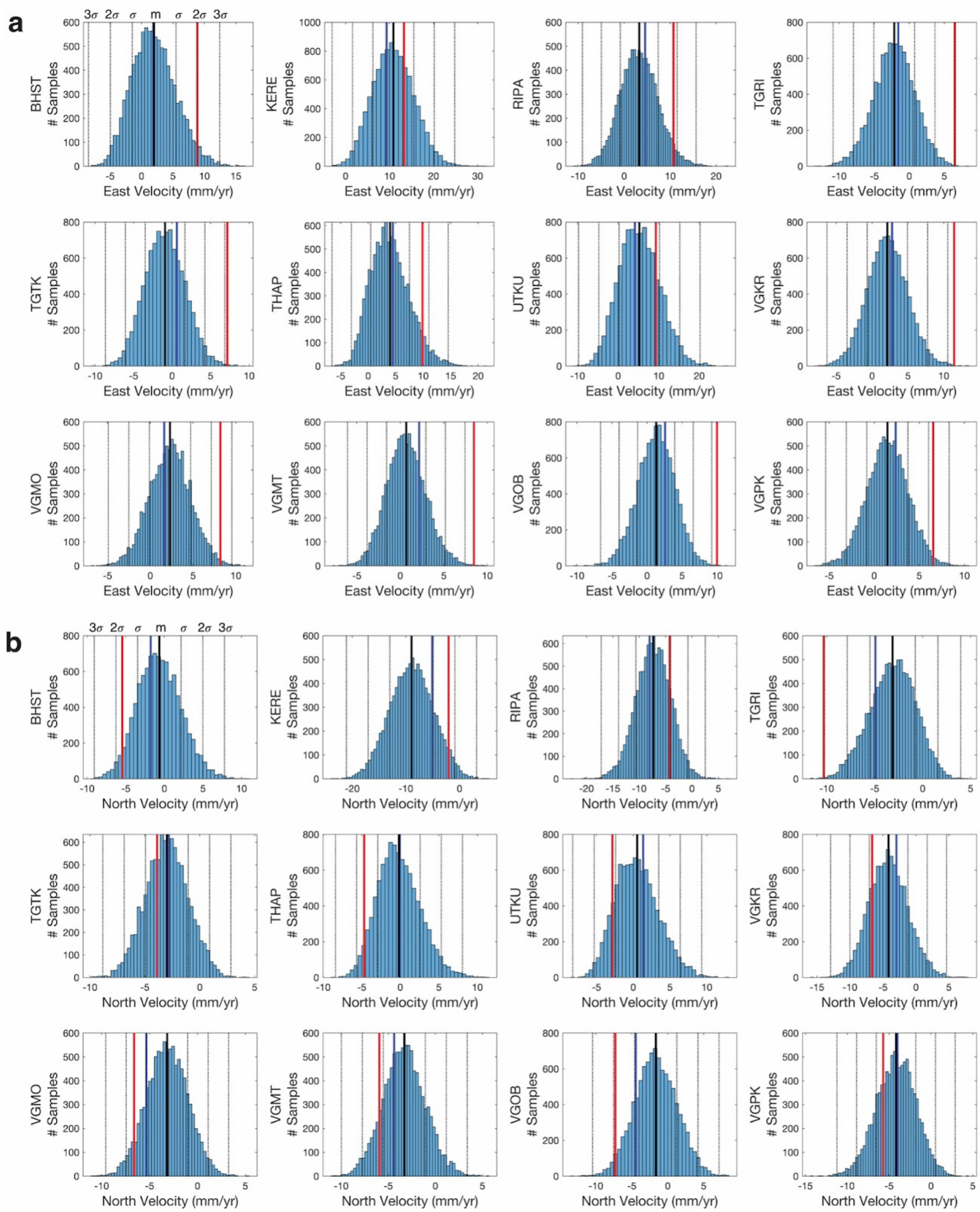

Figure S9. Histogram of velocities obtained by random decomposition of the time series of the deep mid- to long-term SSEs with known tremor periods removed. For the decomposition, we randomly selected times of tremor clusters with the same number of clusters and durations as that which occurs during the deep SSEs. The mean of the distribution is indicated by a solid black line whereas the σ, 2σ, and 3σ of the distribution are indicated by dashed lines. The red and blue lines indicate the averaged velocities obtained respectively for the tremor and inter-tremor periods. a) East velocity. b) North velocity.

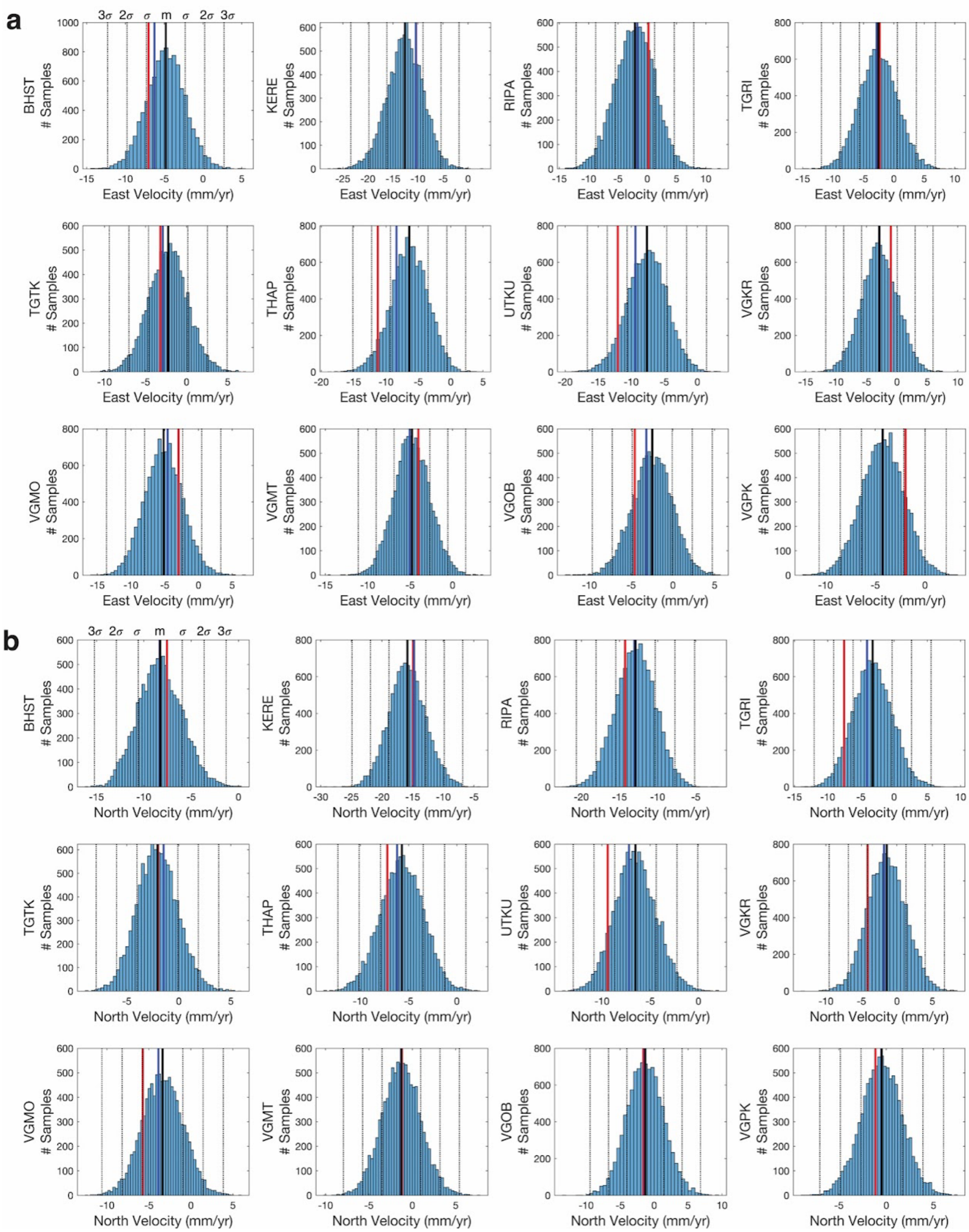

Figure S10. Histogram of velocities obtained by random decomposition of the time series of inter-SSEs with known tremor periods removed. For the decomposition, we randomly selected times of tremor clusters with the same number of clusters and durations as that which occurs during the inter-SSEs. The mean of the distribution is indicated by a solid black line whereas the σ, 2σ, and 3σ of the distribution are indicated by dashed lines. The red and blue lines indicate the averaged velocities obtained respectively for the tremor and inter-tremor periods. a) East velocity. b) North velocity.

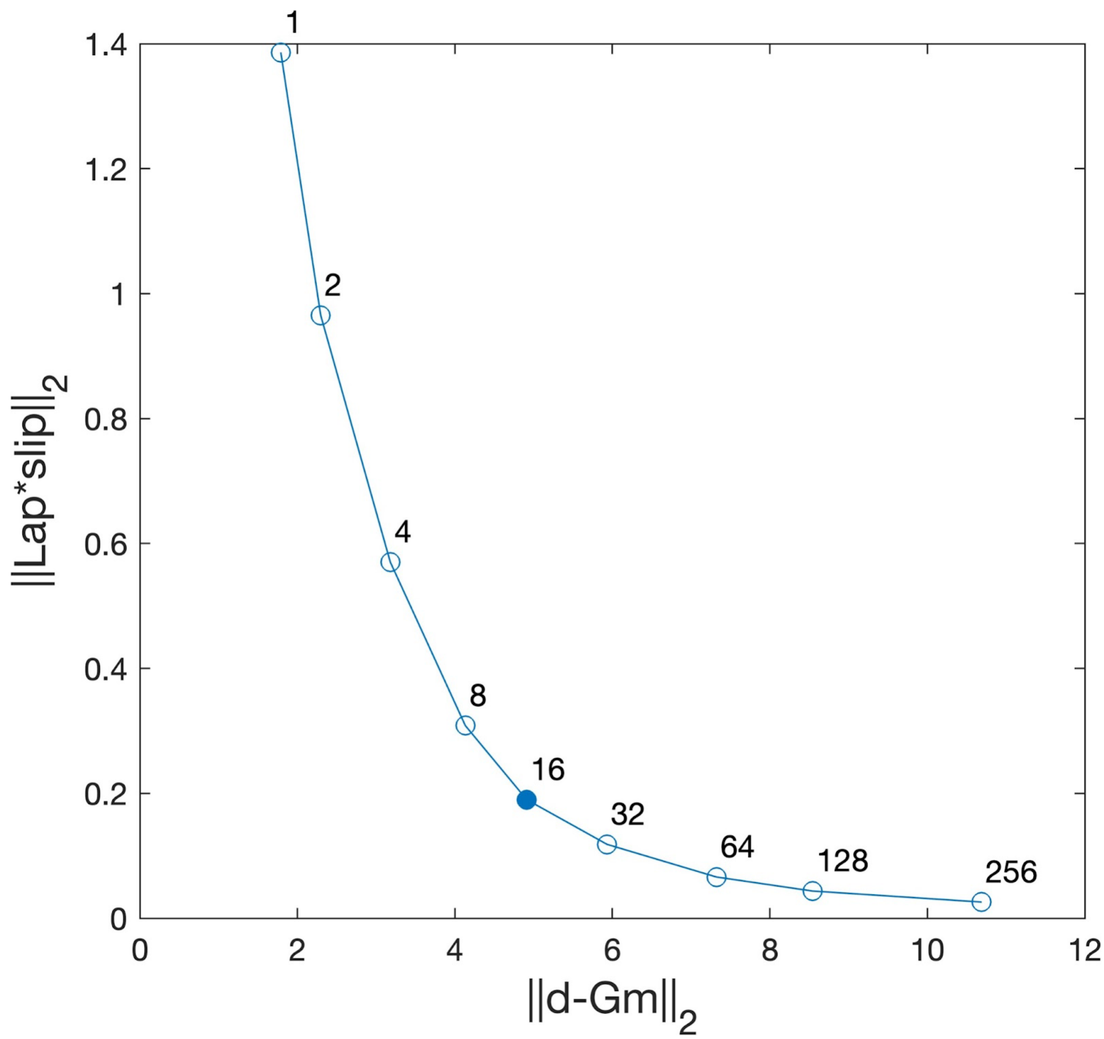

Figure S11. L-curve used to select the smoothing parameter γ where the y-axis is the 2-norm of the discrete Laplacian of the slip rate distribution and the x-axis is the 2-norm of the residuals. Numbers represent values of the smoothing parameter with 16 being the selected value.

Table S1. Summary of deep, ETS-like events in the Manawatu-Kaimanawa region detected through decomposition.

	Max Slip Rate (mm/yr)	Cumulative Moment Rate (Nm/yr)	Average Duration of Tremor Bursts (days)	Average Moment per Tremor Burst (Nm)	Average Equivalent M_W per Tremor Burst
All Tremor	51	2.4×10^{19}	23	1.5×10^{18}	5.0
Tremor during SSEs	80	3.4×10^{19}	32	3.0×10^{18}	5.2
Tremor during Inter-SSEs	25	9.4×10^{18}	17	4.4×10^{17}	4.6